

Rock physics analysis of well-log data

Qi Hu, Kris Innanen, and Marie Macquet

ABSTRACT

We present a rock physics workflow based on the soft-sand model to convert reservoir properties (e.g., porosity, lithology, fluid saturation, and pressure) to seismic elastic attributes (e.g., velocity, density, and modulus) at the CaMI Field Research Station, Alberta, Canada. This model is selected based on the geological setting of the study region and its visible fit to the well-log data. We use the constructed rock physics model to predict the shallow section of velocity and density logs which is missing. The result shows a good agreement with the local geology. We further carry out sensitivity studies for the estimation of reservoir properties from seismic attributes. This is a nonlinear inverse problem and we solve it using a directed Monte-Carlo method (neighborhood algorithm). Various input data parameterizations and model parameterizations are considered. We illustrate that most reservoir properties are difficult to estimate when the inversion system is underdetermined with non-unique solutions. To obtain accurate estimates, it is best to include enough input data or focus on limited solid and fluid phases by making appropriate assumptions on the others. Because the rock physics model used in the study is validated using well data, our analysis should be applicable to the regional area centered on the well.

INTRODUCTION

The CaMI Field Research Station (FRS) is located in Newell County, southwest of Brooks, Alberta. The injection of CO₂ at this pilot site at a shallow depth of approximately 300 meters is designed to simulate leakage of CO₂ from a deeper and larger CO₂ storage project (Lawton et al., 2019). The FRS is now at the early phase of its life-cycle of monitoring CO₂ injection. Different geophysical data have already been acquired to characterize the subsurface and will be used as baselines for the monitoring of CO₂ injection (Macquet et al., 2019).

The Countess 10-22 well was drilled to a depth of 550 m to characterize the overburden and the underburden within the FRS (Lawton et al., 2019). This well has subsequently been completed as an injection well. The shallow stratigraphy is composed of approx. 1000 m of interbedded sandstone and shale-dominated strata of Cretaceous age. The stratigraphic succession of the Upper Cretaceous strata is shown in Figure 1. The Basal Belly River Sandstone (BBRS) injection zone is at a depth of 295 m below ground surface and it is a 7-m-thick fine to medium-grained sandstone. The overlying sealing succession of the storage complex is composed of interbedded mudstone, fine-grained sandstone, and uncleated coals that directly overlies the injection zone. Together, the potential top seal has a combined average net thickness of 225 m in the study area.

A comprehensive log suite including a dipole sonic log was acquired at the Countess 10-22 well. Figure 2 plots the well logs for P-wave velocity (V_P), S-wave velocity (V_S), and density (ρ), of the range 223-535 m. To construct the logs in the shallow section (0-223 m), previous efforts (Eaid et al., 2020) adopt the V_P log of an offset well and then use regres-

sions of V_P to obtain V_S and ρ . However, this approach tends to overestimate the correlation between V_P and ρ as well as the V_S values near the surface (0-50 m). The wireline logs of the injection well (e.g., gamma ray, resistivity, dipole sonic and bulk density) were studied using Schlumberger's elemental log analysis (ELAN) that provided calculated depth profiles, starting from 12 m, of effective porosity, permeability, and rock fraction composition (Swager, 2015). In Figure 3, the interpreted porosity and solid composition logs are plotted

The main goal of this study is to build a regional rock physics model that links the rock properties in Figure 3 to the elastic parameters in Figure 2. Once the rock physics model is validated at the well, it can be used to construct the shallow sections of the V_P , V_S and ρ logs. In addition, it allows us to examine parameter resolution issues for the estimation of rock properties from elastic parameters. The paper is organized as follows. First, we illustrate the forward problem, which is to build a rock physics model to link elastic and rock physics properties. Second, we carry out inversion tests to examine the sensitivity of different rock physics properties with respect to various input data parameterizations.

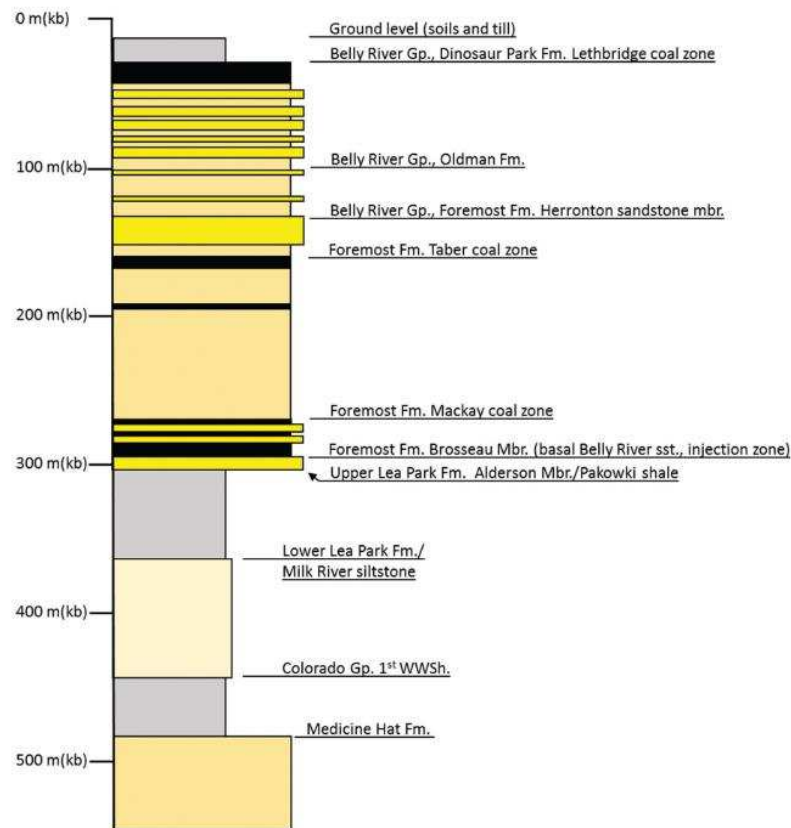


FIG. 1. Stratigraphic succession in the Countess 10-22 well (Lawton et al., 2019).

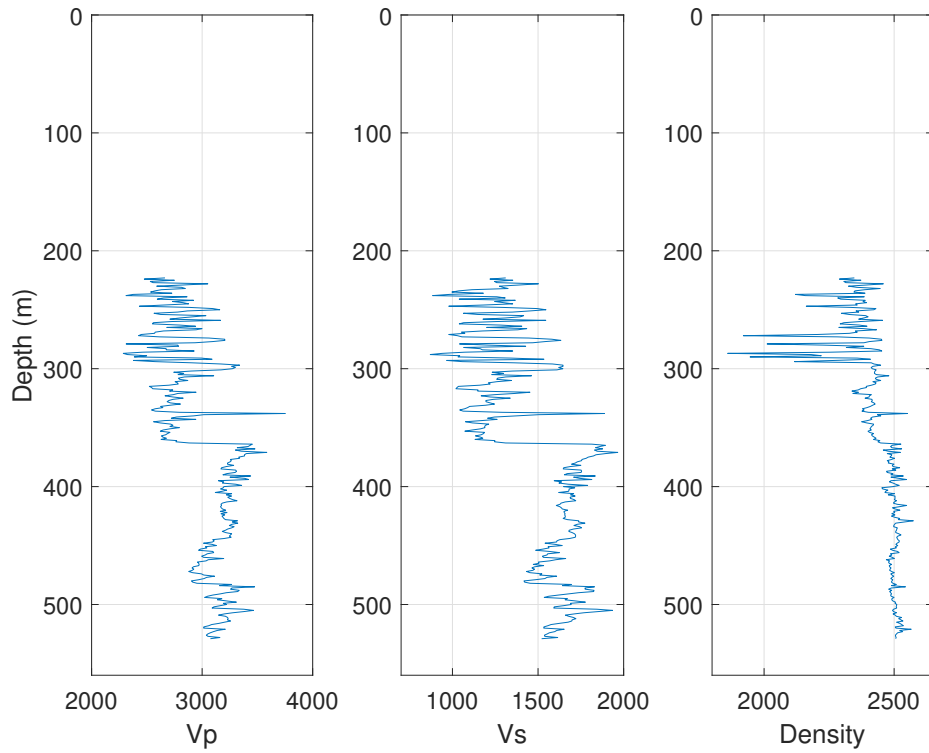


FIG. 2. P-wave velocity (V_P), S-wave velocity (V_S), and density (ρ) logs of the injection well.

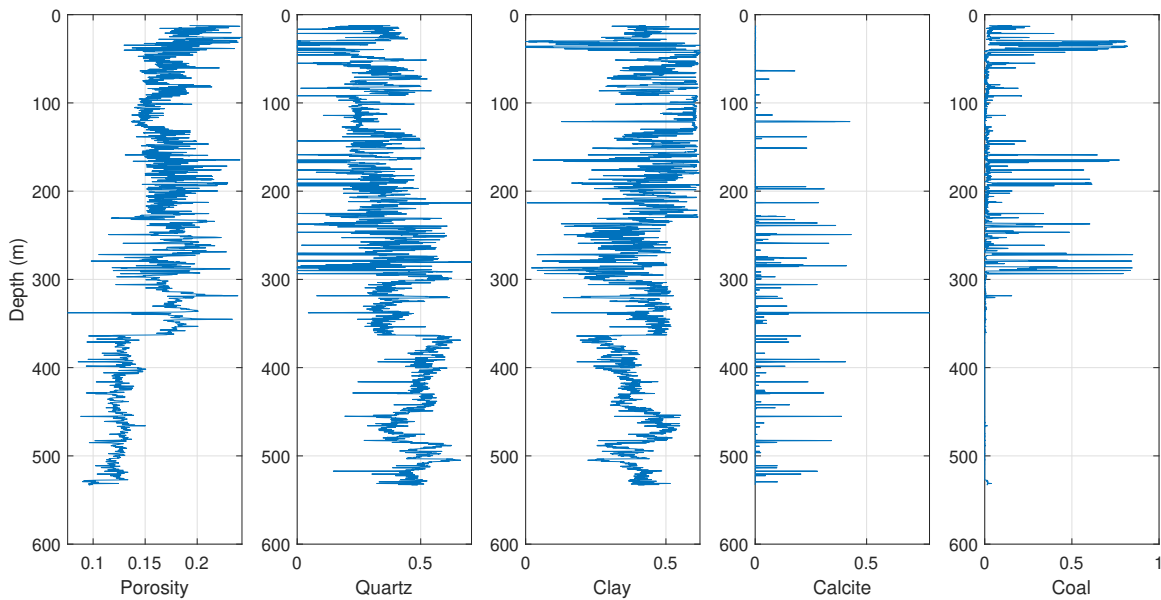


FIG. 3. Porosity and Lithology extracted from the ELAN logs. From left to right: Porosity and the volume fractions of quartz, clay, calcite, and coal.

ROCK PHYSICS MODELING

A significant number of rock physics models have been developed, based on experimental data or physical theories or both, to relate the elastic properties of rock to porosity, mineralogy and pore fluid (Dvorkin, 2004). The rock physics model to be used in interpretation generally depends on the geologic environment. Granular media models based on Hertz-Mindlin contact theory are generally applied in reservoir with sand and shale formations, whereas inclusion models are often used in carbonate reservoirs (Grana, 2016). In the proposed approach, we use the soft-sand model combined with Gassmann's equations and the density equation.

Method

The soft-sand model intends to heuristically describe the elastic behavior of a pack of identical elastic spheres where porosity reduction is due to the introduction of non-cementing particles into the pore space. The soft-sand model connects two endpoints in the elastic modulus versus porosity plane. The zero-porosity endpoint has the bulk and shear moduli of the solid phase K_0 and G_0 , which is calculated according to Voigt–Reuss–Hill average (Hill, 1952):

$$\begin{aligned} K_0 &= \frac{1}{2} \left[\sum_{i=1}^N f_i K_i + \left(\sum_{i=1}^N f_i / K_i \right)^{-1} \right], \\ G_0 &= \frac{1}{2} \left[\sum_{i=1}^N f_i G_i + \left(\sum_{i=1}^N f_i / G_i \right)^{-1} \right], \end{aligned} \quad (1)$$

where N is the number of mineral components, f_i , K_i , and G_i are the volume fraction, bulk modulus, and shear modulus of the i th mineral component, respectively. Hertz-Mindlin grain-contact theory provides an estimation of the bulk and shear moduli of a dry rock, under the assumption that the rock frame is a random pack of spherical grains, subject to an effective pressure P_e , with a given porosity, and an average number of contacts per grain n (coordination number). In the soft sand model, Hertz-Mindlin equations are used to compute the bulk and shear moduli of the dry-rock K_{HM} and G_{HM} at the critical porosity ϕ_c :

$$\begin{aligned} K_{\text{HM}} &= \left[\frac{n^2(1 - \phi_c)^2 G_0^2}{18\pi^2(1 - v_0)^2} P_e \right]^{1/3}, \\ G_{\text{HM}} &= \frac{2 + 3f - v_0(1 + 3f)}{5(2 - v_0)} \left[\frac{3n^2(1 - \phi_c)^2 G_0^2}{2\pi^2(1 - v_0)^2} P_e \right]^{1/3}, \end{aligned} \quad (2)$$

where v_0 is the Poisson's ratio of the solid phase, and f is the degree of adhesion between the grains. We estimate coordination number as $n = 30 - 34\phi + \phi^2$ (Macquet et al., 2019). ϕ is porosity. Then, for $\phi \in (0, \phi_c)$, the bulk and shear moduli K_{dry} and G_{dry} of the dry-rock are estimated by interpolating the elastic moduli at zero porosity and at critical porosity using the modified Hashin-Shtrikman lower bounds:

$$K_{\text{dry}} = \left(\frac{\phi/\phi_c}{K_{\text{HM}} + 4/3G_{\text{HM}}} + \frac{1 - \phi/\phi_c}{K_0 + 4/3G_{\text{HM}}} \right)^{-1} - 4/3G_{\text{HM}},$$

$$G_{\text{dry}} = \left(\frac{\phi/\phi_c}{G_{\text{HM}} + \xi} + \frac{1 - \phi/\phi_c}{G_0 + \xi} \right)^{-1} - \xi, \quad (3)$$

where

$$\xi = \frac{G_{\text{HM}}}{6} \frac{9K_{\text{HM}} + 8G_{\text{HM}}}{K_{\text{HM}} + 2G_{\text{HM}}}. \quad (4)$$

According to Gassmann's equations, the shear modulus of the saturated rock G_{sat} is the same as that of the dry rock, and the bulk modulus of the saturated rock K_{sat} is given by:

$$K_{\text{sat}} = K_{\text{dry}} + \frac{(1 - K_{\text{dry}}/K_0)^2}{\phi/K_f + (1 - \phi)/K_0 - K_{\text{dry}}/K_0^2}$$

where K_f is the bulk modulus of the fluid phase and is calculated using the Brie's fluid mixing equation:

$$K_f = (K_{\text{liquid}} - K_{\text{gas}})(1 - S_{\text{gas}})^3 + K_{\text{gas}}, \quad (5)$$

where K_{gas} is the gas bulk modulus, $K_{\text{liquid}} = (S_{\text{water}}/K_{\text{water}} + S_{\text{oil}}/K_{\text{oil}})^{-1}$ is the liquid bulk modulus given by the Reuss average. The density of the saturated rock is computed as a weighted average of the densities of mineral and fluid components:

$$\rho = (1 - \phi) \sum_{i=1}^N f_i \rho_i + \phi \sum_{i=1}^M f'_i \rho'_i, \quad (6)$$

where ρ_i and ρ'_i are the density of the i th mineral component and the density of the i th fluid component, respectively. The velocities as functions of the elastic moduli and density are then

$$V_P = \sqrt{\frac{K_{\text{sat}} + \frac{4}{3}G_{\text{sat}}}{\rho}}, \quad V_S = \sqrt{\frac{G_{\text{sat}}}{\rho}}. \quad (7)$$

Application

Based on the lithology interpretation result in Figure 3, we consider four mineral components: quartz, clay, calcite and coal. Their volume fractions are denoted by V_{qu} , V_{cl} , V_{ca} , and V_{co} , respectively. We consider two fluid components: water and CO_2 , even if the CO_2 saturation (S_{CO_2}) can be assumed 0 for the Countess 10-22 well (Macquet et al., 2019) because the log suite was acquired before injection. We also take into account the pressure effect and include effective pressure (P_{eff}) as a variable. Therefore, combining Equations (1)-(7), we built a rock physics model with 6 variables (since $V_{\text{co}} = 1 - V_{\text{qu}} - V_{\text{cl}} - V_{\text{ca}}$):

$$(V_P, V_S, \rho) = f(\phi, V_{\text{qu}}, V_{\text{cl}}, V_{\text{ca}}, S_{\text{CO}_2}, P_{\text{eff}}). \quad (8)$$

The predicted velocity and density logs match the real one closely (Figure 4), with an average relative error of 3.4% for V_P , 5.5% for V_S , and 1% for ρ . The rock physics are then used to construct the shallow section (0-223m) of logs. We observe two favorable features in the result. First, the velocities decrease as they approaches the surface, which is geologically meaningful. Second, the variation of V_P , V_S , and for ρ are consistent with the stratigraphic succession in this well, especially at the coal zone.

Table 1. Rock physics parameters used in this study

Parameter	Value	Parameter	Value
Quartz bulk modulus	37 GPa	Coal bulk modulus	8 GPa
Quartz shear modulus	44 GPa	Coal shear modulus	3 GPa
Quartz density	2.65 g/cm ³	Coal density	2 g/cm ³
Clay bulk modulus	25 GPa	Water bulk modulus	2.2 GPa
Clay shear modulus	9 GPa	Water density	1 g/cm ³
Clay density	2.6 g/cm ³	CO ₂ bulk modulus	0.01 GPa
Calcite bulk modulus	76.8 GPa	CO ₂ density	0.4 g/cm ³
Calcite shear modulus	32 GPa	Critical porosity	0.36
Calcite density	2.71 g/cm ³	Degree of adhesion	0.5

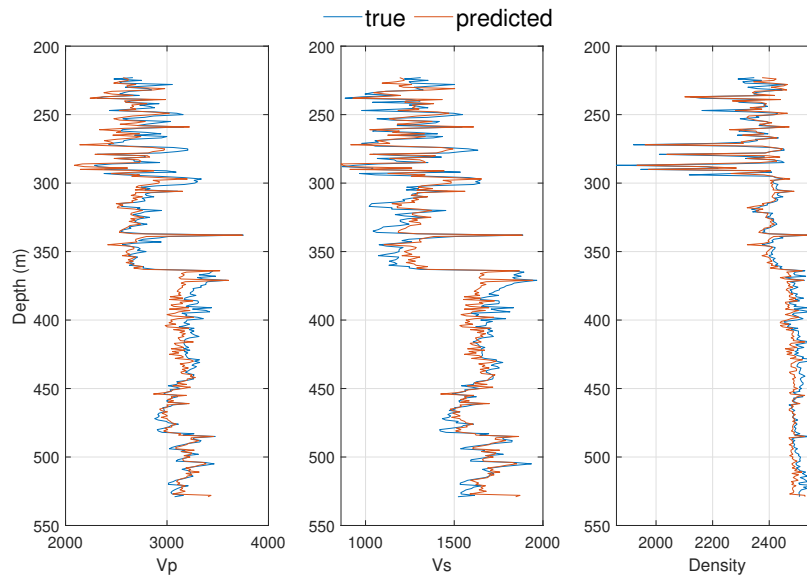


FIG. 4. Predicted velocity and density logs versus real logs

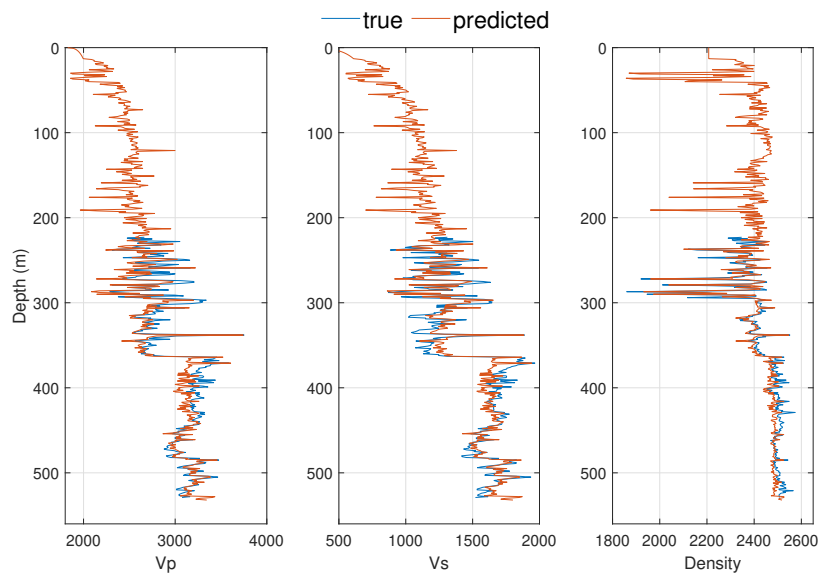


FIG. 5. Constructing the shallow section (0-223 m) of V_P , V_S , and ρ logs.

ROCK PHYSICS INTERPRETATION

Quantitative estimation of rock-physics properties is of great importance for reservoir characterization. In seismic reservoir characterization, the estimation of rock and fluid properties is generally achieved in two steps: seismic inversion and rock physics inversion (Bosch et al., 2010; Grana, 2016; Dupuy et al., 2016a,b). In seismic inversion, we invert the seismic data (e.g., amplitude, time, waveforms) for models of elastic attributes. In rock-physics inversion, we use the realizations of elastic attributes to estimate useful reservoir properties (Doyen, 2007).

The estimation of rock physics properties is not a trivial task because most rock physics models are nonlinear. However, before we adopt a complex inversion algorithm, we should examine if there is a regression relationship between the data and the model. In Figure 6, we crossplot the log data for different elastic-rock physics combinations. Their correlation coefficients are shown on the top of the panel. We observe that most rock physics variables are poorly correlated with either velocity or density, making them difficult to estimate using regressions. The only variable that can be recovered this way is porosity, which has a high correlation with velocities. Even so, it is still necessary to examine if a theory-guide approach can give better results. We can also tell that the correlation between any two rock physics variables are poor, or else they would have similar correlation with the same elastic parameter. Therefore, we are not able to reduce the number of variables using their interdependence.

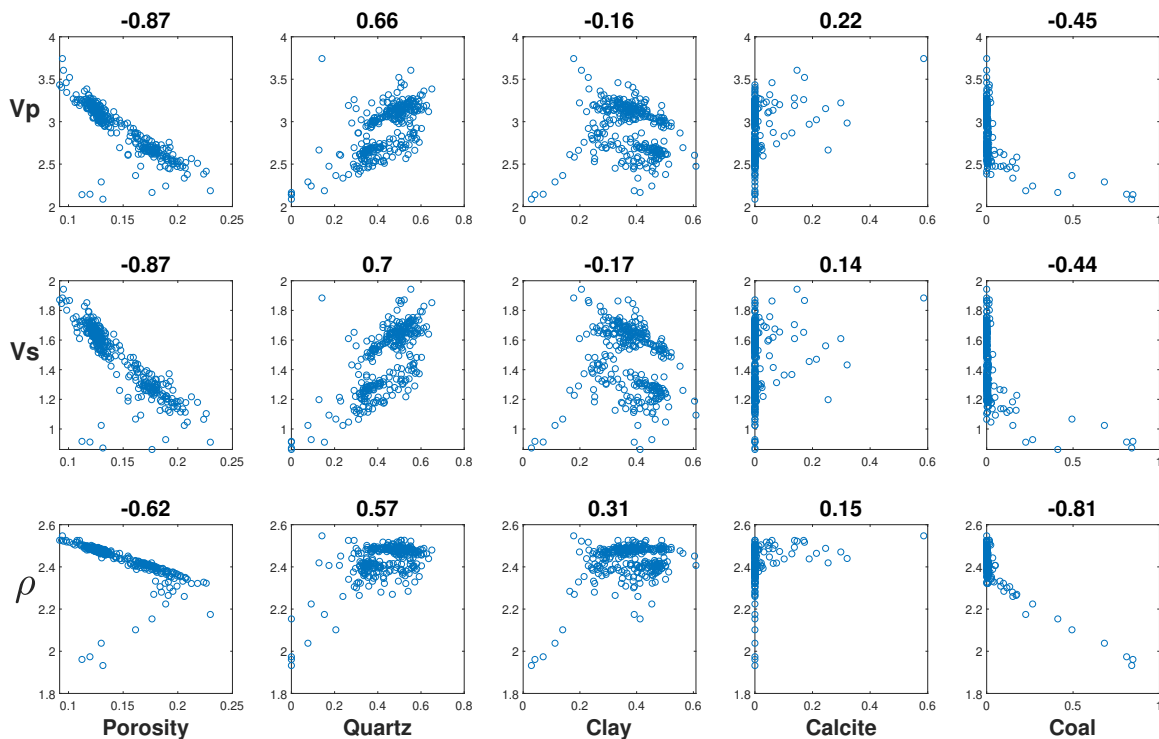


FIG. 6. Scatter plots of elastic parameters against rock physics parameters. Well-log data are used. The correlation between two variables is shown on the top of the panel.

Method

The inverse problem consists in the extraction of models (rock physics parameters) from input data (elastic attributes) and is formulated as

$$\mathbf{d} = f(\mathbf{m}). \quad (9)$$

As illustrated in Equation 8, the model vector \mathbf{m} comprises of six rock physics parameters: porosity, CO₂ saturation, effective pressure, and volume fractions of quartz, clay, and calcite; the data vector comprises of V_P, V_S , and ρ ; the function f is the rock physics model.

The optimization aims to minimize a scalar function (misfit function) describing the discrepancy between the observed data \mathbf{d}_{obs} and calculated data $f(\mathbf{m})$ (by forward modeling). We use the L_2 norm to compute the misfit as

$$E(\mathbf{m}) = \frac{1}{2}[(\mathbf{d}_{\text{obs}} - f(\mathbf{m}))^T C_d^{-1}(\mathbf{d}_{\text{obs}} - f(\mathbf{m}))], \quad (10)$$

where C_d^{-1} is the data covariance matrix, which contains information on data uncertainties.

We use a global optimization method: the neighborhood algorithm (NA). It belongs to the category of directed Monte Carlo methods. Unlike the uniform Monte Carlo method, which by definition is a completely blind search since each new sample is independent of the previous samples, the neighborhood algorithm makes use of previous samples to guide their search Sambridge (1999).

To make a search for new models be best guided by all previous models, NA makes use of the geometrical constructs known as Voronoi cells to derive the search in model space. Each cell is simply the nearest neighbor region about one of the previous samples. For example, the Voronoi cell about point \mathbf{m}_i is given by

$$V(\mathbf{m}_i) = \{\mathbf{x} | \|\mathbf{x} - \mathbf{m}_i\|_2 \leq \|\mathbf{x} - \mathbf{m}_j\|_2 \text{ for } j \neq i\}. \quad (11)$$

The algorithm uses the spatial properties of Voronoi cells to directly guide the sampling of parameter space. It can be summarized in four steps:

- 1) Generate an initial set of n_s models uniformly (or otherwise) in parameter space;
- 2) Calculate the misfit function for the most recently generated set of n_s models and determine the n_r models with the lowest misfit of all models generated so far;
- 3) Generate n_s new models by performing a uniform random walk in the Voronoi cell of each of the n_r chosen models (i.e. n_s/n_r samples in each cell);
- 4) Go to step 2.

The philosophy behind the algorithm is that the misfit of each of the previous models is representative of the region of space in its neighborhood (defined by its Voronoi cell). Therefore at each iteration new samples are concentrated in the neighborhoods surrounding the better data-fitting models. In this way the algorithm exploits the information contained in the previous models to adapt the sampling.

Numerical Examples

We study the sensitivity of rock physics parameters with respect to three data parameterizations: (V_P) , (V_P, V_S) , and (V_P, V_S, ρ) . Also, we consider different realistic model parameterizations.

Cases:

- 1) 6 unknowns: porosity (ϕ) + 4 minerals ($V_{qu}, V_{cl}, V_{ca}, V_{co}$) + 2 fluids (S_{co_2}, S_w);
- 2) 4 unknowns: porosity (ϕ) + 4 minerals ($V_{qu}, V_{cl}, V_{ca}, V_{co}$) + 1 fluid (S_w).
- 3) 3 unknowns: porosity (ϕ) + 2 minerals (V_{qu}, V_{cl}) + 2 fluids (S_{co_2}, S_w).
- 4) 2 unknowns: porosity (ϕ) + 2 minerals (V_{qu}, V_{cl}) + 1 fluid (S_w).
- 5) 2 unknowns: porosity (ϕ) + 1 mineral (V_{qu}) + 2 fluids (S_{co_2}, S_w).

In these cases, we assign random values to the rock physics properties. The data are computed with the same algorithm (i.e., the rock physics model in Equation 8) for observed and computed data in inversion. We first run tests from case 1 to case 5 with the exact input data. We then repeat case 5 using erroneous data.

We find:

- a) If the number of model parameters is larger than the number of data, the inversion system is underdetermined with non-unique solutions (case 1, case 2, and cases 3-5 with only V_P as input). In these cases, repeating the test always leads to a different solution, depending on which one is randomly picked. As a result, none of the model parameters can be accurately estimated. The major focus in this problem should be which parameter is relatively stable.
- b) The estimation is very accurate as soon as the system is not underdetermined, such as the estimation of (ϕ, V_{cl}, S_{co_2}) from (V_P, V_S, ρ) in case 3, the estimation of (ϕ, V_{cl}) from (V_P, V_S) in case 4, and the estimation of (ϕ, S_{co_2}) from (V_P, V_S) in case 5. Although (V_P, V_S) is enough to estimate two model parameters, adding density improves the convergence.
- c) In Figure 12, although V_S and ρ are erroneous, including them as input data can still largely reduce the uncertainty in rock physics interpretation (a motivation to choose elastic inversion over acoustic inversion).

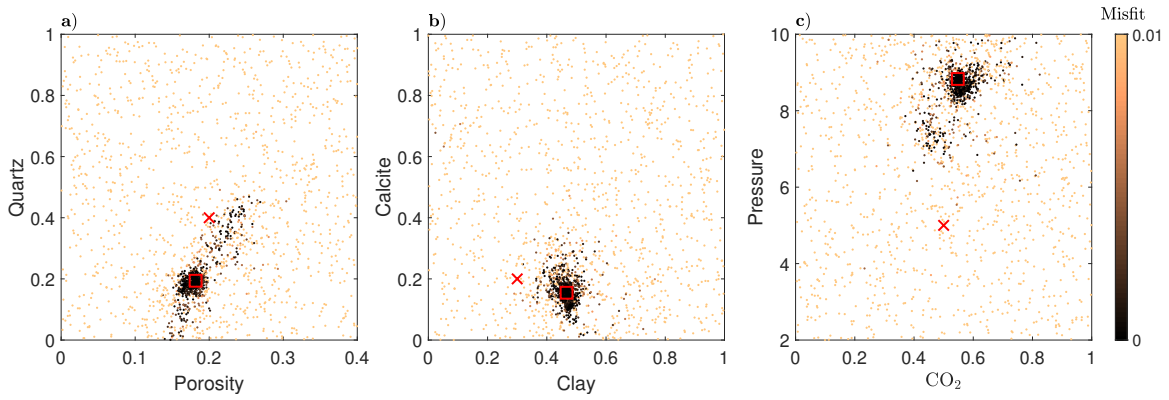


FIG. 7. Case 1: Inversion of 6 parameters from (V_P, V_S, ρ) . Red cross: true model. Red square: inverted model

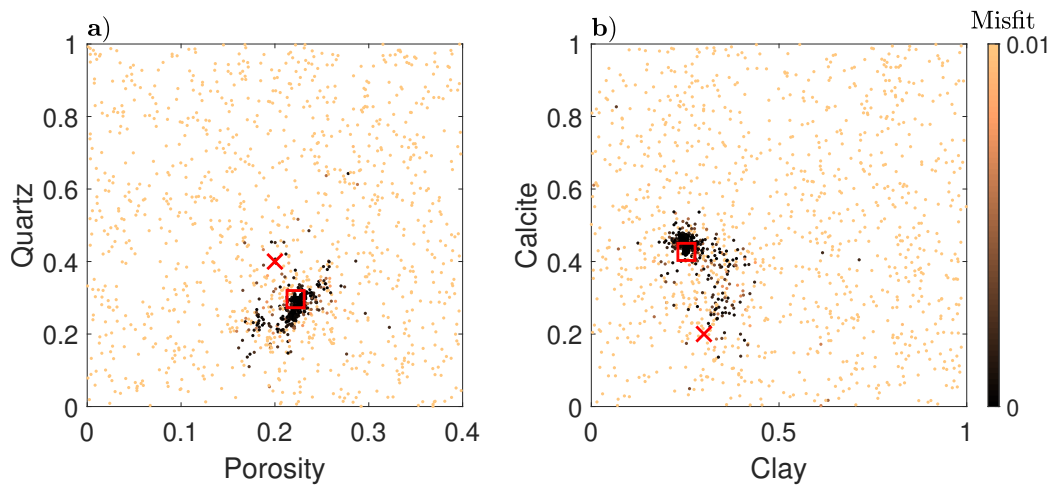


FIG. 8. Case 2: Inversion of porosity and the volume fractions of quartz, clay, and calcite from (V_P, V_S, ρ) .

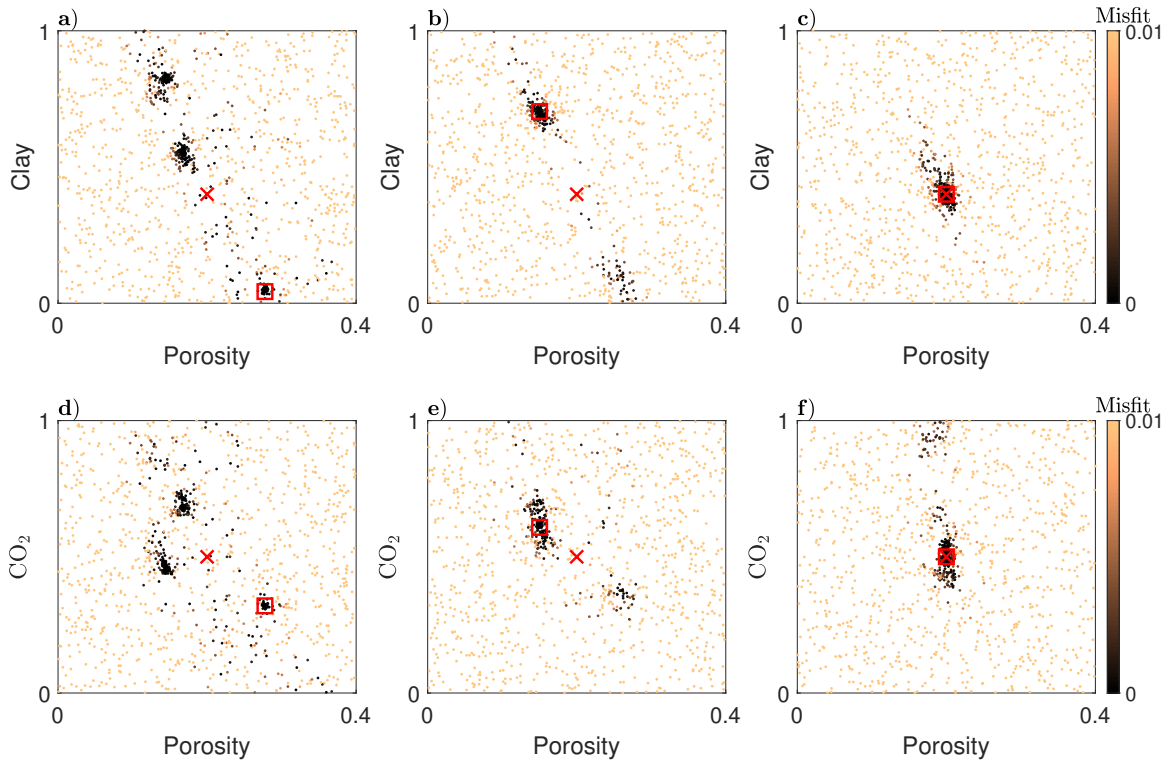


FIG. 9. Case 3: Inversion of porosity, clay content, and CO₂ saturation from (a, d) V_P , (b, e) V_P , V_S , and (c, f) V_P , V_S , ρ .

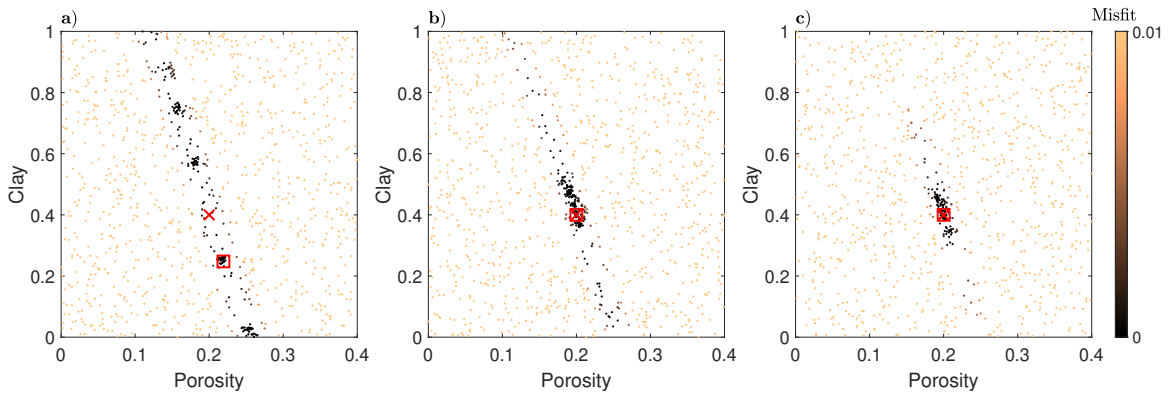


FIG. 10. Case 4: Inversion of porosity and clay content from (a) V_P , (b) V_P , V_S , and (c) V_P , V_S , ρ .

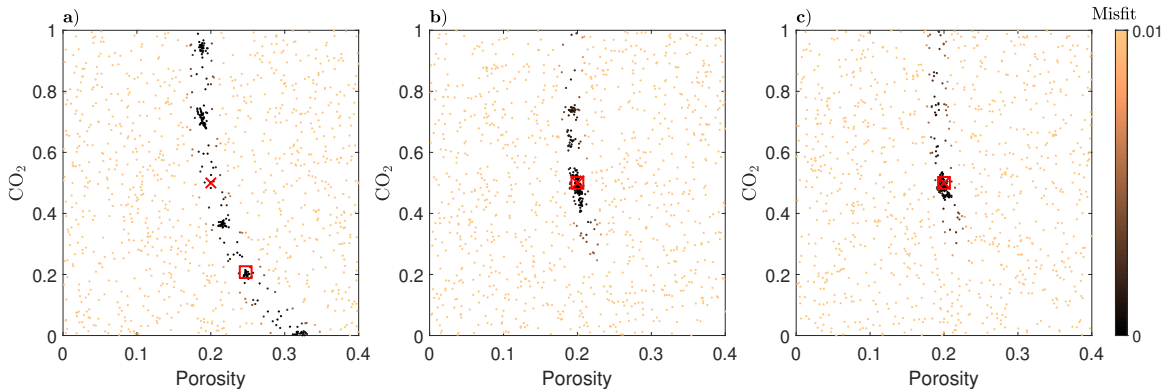


FIG. 11. Case 5: Inversion of porosity and CO₂ saturation from (a) V_P , (b) V_P , V_S , and (c) V_P , V_S , ρ .

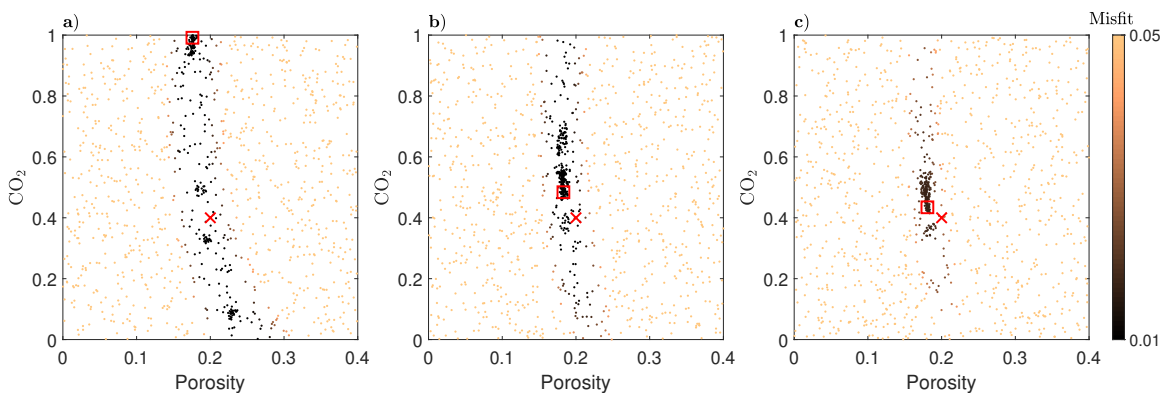


FIG. 12. Repeat Case 5 but add 5% error to V_P , V_S , and 10% error to ρ

CONCLUSIONS

In this study we provide a rock physics model to link the elastic and rock physics properties at the CaMI FRS. The model is validated using the data of the Countess 10-22 well. We then use the rock physics model to predict velocity and density logs near the surface. The result could provide data for establishing low frequency model for seismic inversion. Moreover, based on the rock physics model, we carry out sensitivity studies for the estimation of reservoir properties from seismic attributes. We illustrate that it is difficult to obtain accurate estimates when the inversion system is underdetermined. Therefore, it is important to include enough input data by running elastic seismic inversion.

ACKNOWLEDGMENTS

We thank the sponsors of CREWES for continued support. This work was funded by CREWES industrial sponsors and NSERC (Natural Science and Engineering Research Council of Canada) through the grant CRDPJ 543578-19. The data were acquired through a collaboration with the Containment and Monitoring Institute, Carbon Management Canada. The first author was partially supported by a scholarship from the SEG Foundation.

REFERENCES

- Bosch, M., Mukerji, T., and Gonzalez, E. F., 2010, Seismic inversion for reservoir properties combining statistical rock physics and geostatistics: A review: *Geophysics*, **75**, No. 5, 75A165–75A176.
- Doyen, P., 2007, *Seismic reservoir characterization: An earth modelling perspective*: EAGE publications.
- Dupuy, B., Garambois, S., Asnaashari, A., Balhareth, H. M., Landrø, M., Stovas, A., and Virieux, J., 2016a, Estimation of rock physics properties from seismic attributes — Part 2: Applications: *Geophysics*, **81**, No. 4, M55–M69.
- Dupuy, B., Garambois, S., and Virieux, J., 2016b, Estimation of rock physics properties from seismic attributes — Part 1: Strategy and sensitivity analysis: *Geophysics*, **81**, No. 3, M35–M53.
- Dvorkin, J., 2004, Seismic reflections of rock properties: *Hart's E & P*, **77**, No. 11, 59–61.
- Eaid, M., Keating, S., Macquet, M., and Innanen, K., 2020, Elastic FWI of the CAMI FRS 3d walkaway-walkaround VSP fiber survey: A synthetic case study: CREWES Report.
- Grana, D., 2016, Bayesian linearized rock-physics inversion: *Geophysics*, **81**, No. 6, D625–D641.
- Hill, R., 1952, The elastic behaviour of a crystalline aggregate: *Proceedings of the Physical Society. Section A*, **65**, No. 5, 349.
- Kuster, G. T., and Toksöz, M. N., 1974, Velocity and attenuation of seismic waves in two-phase media: *Geophysics*, **39**, No. 5, 587–618.
- Lawton, D. C., Dongas, J., Osadetz, K., Saeedfar, A., and Macquet, M., 2019, Development and analysis of a geostatic model for shallow CO₂ injection at the field research station, southern alberta, canada: *Geophysics and Geosequestration*. Cambridge University Press, Cambridge, **280**, 296.
- Macquet, M., Lawton, D. C., Saeedfar, A., and Osadetz, K. G., 2019, A feasibility study for detection thresholds of co₂ at shallow depths at the camo field research station, newell county, alberta, canada: *Petroleum Geoscience*, **25**, No. 4, 509–518.
- Sambridge, M., 1999, Geophysical inversion with a neighbourhood algorithm—i. searching a parameter space: *Geophysical journal international*, **138**, No. 2, 479–494.
- Swager, L., 2015, Geophysical log descriptive report: CMCRI COUNTSS 10-22-17-16 ELAN: Schlumberger Carbon Services-CS1512-112-LS.